Journal of Power Sources 196 (2011) 7333–7337

Contents lists available at ScienceDirect

Journal of Power Sources

journal homepage: www.elsevier.com/locate/jpowsour

Short communication

# Structure–property relationship in layered perovskite cathode $LnBa_{0.5}Sr_{0.5}Co_2O_{5+\delta}$ (Ln = Pr, Nd) for solid oxide fuel cells

Abul K. Azad*, Jung H. Kim, John T.S. Irvine

*School of Chemistry, University of St. Andrews, KY16 9ST, United Kingdom*

ARTICLE INFO

*Article history:*
Received 25 October 2010
Received in revised form 1 February 2011
Accepted 20 February 2011
Available online 26 February 2011

*Keywords:*
Layered perovskite
Neutron diffraction
Structural phase transition
Electrical conductivity
Area specific resistance

ABSTRACT

The layered cobaltites $LnBa_{0.5}Sr_{0.5}Co_2O_{5+\delta}$ (Ln = Pr, Nd) have been prepared by solid state reaction technique and structure–property relationships were investigated by means of neutron diffraction, ac impedance and dc conductivity measurements. Room temperature neutron diffraction shows the ordered distribution of oxygen vacancies in [$PrO_\delta$] planes which doubles the lattice parameters from the perovskite cell parameter as $a = b \approx 2a_p$, and $c \approx 2a_p$ ($a_p$ is the cell parameter of the simple perovskite) yielding tetragonal symmetry in the *P4/mmm* space group. On heating, the oxygen vacancy ordering disappears and the structure can be defined as $a = b \approx a_p$ and $c \approx 2a_p$ in the same space group. Oxygen occupancies have been determined as a function of temperature from neutron diffraction. It was found that from 573 K to 973 K the total oxygen loss is about 0.265 O/formula unit and 0.366 O/formula unit for Pr and Nd containing materials, respectively. The oxygen occupancy decreases and cell volume increases with increasing temperature. Electrical conductivity measurements in air show that conductivity decreases with temperature, and at 873 K the conductivity is 493 S $cm^{-1}$ and 255 S $cm^{-1}$ for Pr and Nd containing samples, respectively. AC impedance measurements in symmetrical cell arrangement with CGO electrolyte shows that area specific resistance decreases with increasing temperature. At 873 K the ASR is 0.286 Ω $cm^2$ and 1.15 Ω $cm^2$ for Pr and Nd containing samples, respectively.



## 1. Introduction

Cobalt containing perovskite oxides have superior oxygen diffusion kinetics and show unique electronic and magnetic properties as a consequence of the ability of Co to adopt 2+, 3+ and 4+ oxidation states [1–3]. In addition to the spin, charge and orbital degrees of freedom found in the manganite perovskites, the cobaltites are expected to exhibit a degree of freedom in the electronic configuration of the cobalt ion. Layered cobaltites with general formula $LnBaCo_2O_{5+\delta}$ (Ln = lanthanides, $0 < \delta < 1$) have been the subject of several studies during the last years due to their giant magnetoresistance properties (the highest found in cobalt oxides), the spin-state transitions, the interplay of the spin-state with the charge, orbital and metal–insulator transitions [4–9]. More recently, these materials have found to be good to use as cathode materials for solid oxide fuel cells [10–12]. The oxygen content and mobility plays a major role in determining electronic, magnetic and transport properties. The oxygen content also controls the mean valence of Co ions, the coordination of Co (pyramidal or octahedral) and has a strong influence on the spin state of Co. So far, most of the investigations have concentrated on two particular compositions, namely $\delta = 0.0$ and 0.5, for which an ordering of oxygen vacancies possibly exists. In $LnBaCo_2O_5$ ($\delta = 0$) the pyramidal positions are occupied by the same amount of $Co^{2+}$ and $Co^{3+}$ ions. In contrast, in $LnBaCo_2O_{5.5}$ ($\delta = 0.5$) only $Co^{3+}$ ions are present which coexists in ideally alternating octahedral $CoO_6$ and pyramidal $CoO_5$ environments. For low $\delta$, there is great tendency to form charge ordered structures which has been reported for $YBaCo_2O_5$ [4] and $TbBaCo_2O_5$ [5]. Neutron diffraction measurements show that $LnBaCo_2O_5$ ($\delta = 0$) compounds are antiferromagnetic (AFM) with $T_N \sim 340$ K (Ln = Tb, Dy, Ho) [13], ~350 K (*for* Y) [14], ~380 K (*Ln* = Nd) [15]. Metal–insulator and spin-state transitions as well as successive magnetic transitions due to competing ferromagnetic (FM)–antiferromagnetic (AFM) interactions are present in compounds with $\delta = 0.5$ for a wide variety of rare earths [1,6,9,16]. The metal–insulator transition mainly takes place in the temperature range RT to 373 K (depending on Ln), which seems to be related to a spin-state transition of the $Co^{3+}$ ions [1,6,7,9,16–19]. Depending on the oxygen content, $\delta$, several kinds of superstructures have been reported in the literature along with the various possible models of oxygen ordering [1–3,20,21]. Due to the wide range of oxygen non-stoichiometry and a strong tendency of the oxygen ions and vacancies to order, the extra oxygen which is known to fill [$LnO_\delta$] layers, can create complex crystal structures with mixed octahedral and pyramidal cobalt environments.

* Corresponding author. Tel.: +44 1334 463844; fax: +44 1334 463808.
*E-mail address:* aka7@st-andrews.ac.uk (A.K. Azad).

0378-7753/$ – see front matter © 2011 Elsevier B.V. All rights reserved.
doi:10.1016/j.jpowsour.2011.02.063

Recently, several research groups have reported excellent properties of $LnBaCo_2O_{5+\delta}$ as cathode materials for intermediate temperature solid oxide fuel cells (IT-SOFCs) [22–25]. Chang et al. [11] have investigated the electrochemical properties of $GdBaCo_2O_{5+\delta}$ for IT-SOFC applications and reported an ASR value of 0.534 Ω cm$^2$ at 923 K. Kim et al. [12] has reported the oxygen ion diffusivity and surface exchange coefficient of $PrBaCo_2O_{5+\delta}$ to be $10^{-5}$ cm$^2$ s$^{-1}$ and $10^{-3}$ cm s$^{-1}$ respectively, at 623 K.

The main objective of this work is to investigate high temperature structural characteristics and to investigate the structure–property relationships in $LnBa_{0.5}Sr_{0.5}Co_2O_{5+\delta}$ (Ln = Pr, Nd) perovskite cobaltites. From structural data, we have explored the oxygen content and mean valence states of Co at different temperatures (from RT to 973 K). Oxygen vacancy ordering, electrical conductivity and area specific resistance were measured to relate the structural data with physical properties.

## 2. Experimental

Polycrystalline samples of $PrBa_{0.5}Sr_{0.5}Co_2O_{5+\delta}$ (PBSCO) and $NdBa_{0.5}Sr_{0.5}Co_2O_{5+\delta}$ (NBSCO) were prepared by standard solid state reaction. The sample preparation procedure has been described in details elsewhere [25]. Phase purity, identity and homogeneity were confirmed by X-ray powder diffraction (XRPD) using STOE Stadi P transmission diffractometer ($CuK\alpha_1$, λ = 0.15406 nm). High resolution and high intensity time-of-flight neutron powder diffraction (NPD) data were collected as a function of temperature using the GEM diffractometer at the ISIS spallation source at Rutherford Appleton Laboratory, UK. Temperature-dependent neutron diffraction data were collected at 373, 473, 573, 673, 773, 873 and 973 K. The diffraction data sets were analysed using the GSAS package [26].

Polarization behaviour was investigated by measuring the ac impedance response in symmetrical cell geometry. Inks of single-phase cathodes were made by mixing the powders with the appropriate solvent and binder system. The electrodes were then applied on both sides of dense $Ce_{0.9}Gd_{0.1}O_{2-d}$ (GDC91) pellets of 1.5–2.0 mm thick electrolytes using screen printing to form symmetrical half-cells. These were sintered for 1 h at 1273 K to form a porous electrode structure well bounded to the electrolyte. The final electrode area of the symmetrical cell was about 1.09 cm$^2$. The area specific resistances (ASRs) were measured via a.c. impedance using a Schlumberger Solartron 1260 frequency response analyzer coupled with a 1287 electrochemical interface controlled by *Z* plot electrochemical impedance software in the frequency range 0.01 Hz to 1 MHz with an amplitude of 50 mV. The samples were measured in stagnant air from between 573 and 1173 K with 50 K steps. The cathode polarization resistance (Rp) was determined from the difference between low and high frequency intercepts on the real axis of the impedance curves, divided by 2. DC electrical conductivity was measured via a four terminal method using a Keithley 220 current source and a Schlumberger Solartron digital multimeter.

## 3. Results and discussion

### 3.1. Structural studies

Rietveld refinement of room temperature (RT) XRPD and NPD data shows that the structural symmetry of PBSCO and NBSCO are tetragonal in the space group *P4/mmm* (No.123). Fig. 1a shows the Rietveld refinement profile of the room temperature NPD data for PBSCO. The refinement of the structural parameters shows the ordering of oxygen vacancies. Different models and oxygen orderings were considered to explore possible order arrangements of

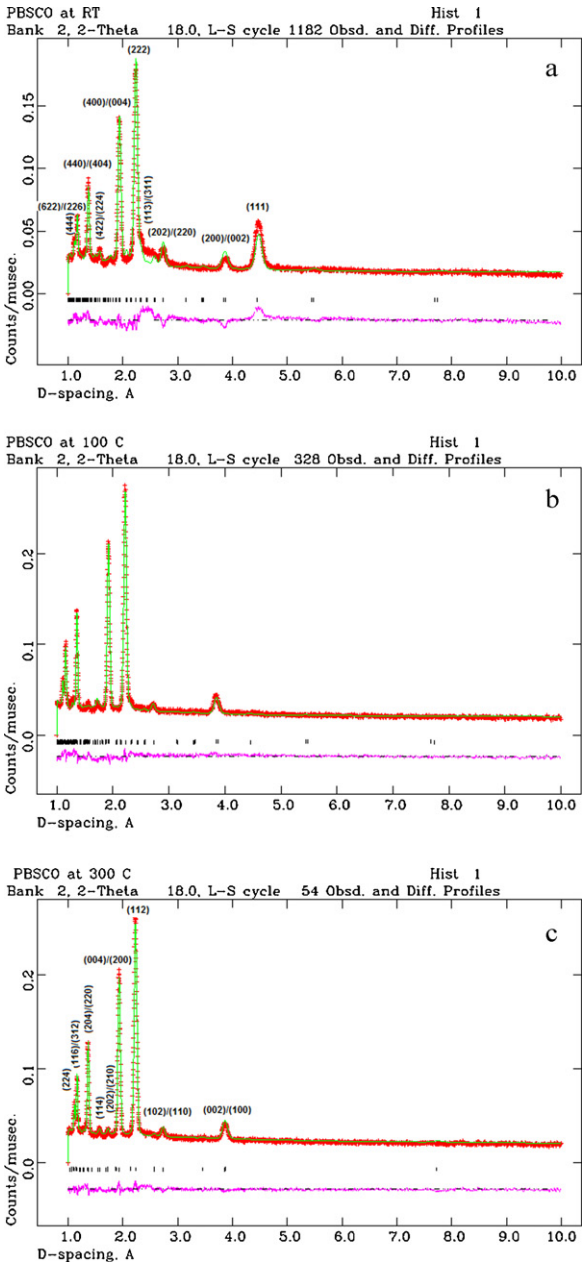


**Fig. 1.** (a–c) Observed (circles) and calculated (continuous line) NPD intensity profiles for $PrBa_{0.50}Sr_{0.5}Co_2O_{5+\delta}$ at RT (a), at 373 K (b) and at 573 K (c) in the *P4/mmm* space group. At RT and 373 K the cell parameters are related as $2a_p \times 2a_p \times 2a_p$ and at 573 K, the cell parameters are related as $a_p \times a_p \times 2a_p$. The short vertical lines indicate the angular position of the allowed Bragg reflections. At the bottom in each figure the difference plot, $I_{obs} - I_{calc}$, is shown.

the oxygen vacancies. The superstructure peaks are attributed to a particular order of oxygen vacancies in the structure and can be indexed by doubling both *a* and *b* lattice parameters. In case of PBSCO, the most intense superstructure peak at room temperature can be indexed as (1 1 1). The selected model corresponds to the *P4/mmm* space group in the setting $2a_p \times 2a_p \times 2a_p$ ($a_p$ is the cell parameter of simple cubic perovskite in the *Pm3m* space group) and with the perfect order in a $2a_p \times 2a_p$ supercell in the [Pr/Nd–$O_\delta$] planes, with vacancies located in the 1*b* (0 0 ½), 1*d* (½ ½ ½) and 2*f* (0 ½0) Wyckoff positions. This model can also index other superstructure reflections corresponding to HHL and HLL (H and L are odd numbers and H ≠ L). Refinement of oxygen occupancies for oxygen sites improved the profile matching. It was observed from

**Table 1**
(a) Main crystallographic information for $PrBa_{0.5}Sr_{0.5}Co_2O_{5.23}$ (space group *P4/mmm*) from NPD data at room temperature in the $2a_p \times 2a_p \times 2a_p$ setting. The cell parameters, $a = 0.77585\ (6)$ nm, $c = 0.7704\ (1)$ nm and the cell volume, $v = 0.46375(3)$ nm$^3$.

| Atoms | Wyckoff position | *x* | *y* | *Z* | *B* | Fractional occupancy |
|---|---|---|---|---|---|---|
| Pr | 4*k* (*x x* 1/2) | 0.2548(3) | 0.2548(3) | 0.5 | 0.011(2) | 1.0 |
| Ba/Sr | 4*j* (*x x* 0) | 0.2411(4) | 0.2411(4) | 0.0 | 0.003(7) | 0.5/0.5 |
| Co1 | 2*g* (0 0 *z*) | 0.0 | 0.0 | 0.2323(3) | 0.007(1) | 1.0 |
| Co2 | 2*h* (½ ½ *z*) | 0.5 | 0.5 | 0.319(2) | 0.007(1) | 1.0 |
| Co3 | 4*i* (0 ½ *z*) | 0.0 | 0.5 | 0.2754(3) | 0.007(1) | 1.0 |
| O1 | 1*a* (0 0 0) | 0.0 | 0.0 | 0.0 | 0.001(8) | 1.0 |
| O2 | 1*c* (½ ½ 0) | 0.5 | 0.5 | 0.0 | 0.004(7) | 1.0 |
| O3 | 2*f* (0 ½ 0) | 0.0 | 0.5 | 0.0 | 0.020(4) | 0.474(3) |
| O4 | 1*b* (0 0 ½) | 0.0 | 0.0 | 0.5 | – | 0.024(5) |
| O5 | 1*d* (½ ½ ½) | 0.5 | 0.5 | 0.5 | 0.035 | 0.0 |
| O6 | 2*e* (0 ½ ½) | 0.0 | 0.5 | 0.5 | 0.010(7) | 1.0 |
| O7 | 8*s* (*x* 0 *z*) | 0.2616(4) | 0.0 | 0.2773(3) | 0.052(3) | 1.0 |
| O8 | 8*t* (*x* ½ *z*) | 0.2585(4) | 0.5 | 0.2444(4) | 0.043(5) | 1.0 |

the refinement that the oxygen position at 1*d* (½ ½ ½) was completely vacant and, 1*b* (0 0 ½) and 2*f* (0 ½0) are partially occupied. The main crystallographic information for $PrBa_{0.5}Sr_{0.5}Co_2O_{5.498}$ (space group *P4/mmm*) from NPD data at room temperature in the $2a_p \times 2a_p \times 2a_p$ setting is given in Table 1. The ordering of the oxygen vacancies in the perovskite matrix is responsible for the superstructure. The oxygen vacancies order within the [Pr–$O_\delta$] layers, resulting in an oxygen-rich and oxygen deficient *a*–*c* layers and consequently in a doubling of the unit cell along *a* and *b* directions [3]. Partial disorder is restricted to a solution with atoms in 1*b* and 2*f* Wyckoff positions of the *P4/mmm* space group. In order to get samples with perfect ordering it is important to make the samples in controlled manner to get oxygen occupancy 5.5.

In PBSCO, the ordering of oxygen vacancies were observed from RT to 473 K. Fig. 1b shows the Rietveld profile at 373 K for PBSCO. At 373 and 473 K, the intensity of the most intense superstructure reflection (1 1 1) was very low but other superstructure reflections like (1 1 3)/(3 1 1) have small intensity. To match the intensities of these reflections we need to consider the unit cell as $2a_p \times 2a_p \times 2a_p$. All the three Wyckoff positions for oxygen at 1*b* (0 0 ½), 1*d* (½ ½ ½) and 2*f* (0 ½0) were partially occupied. In the temperature range 573 K to 973 K, the structure is tetragonal in the *P4/mmm* space group with $a = b \approx a_p$ and $c \approx 2a_p$. Fig. 1c shows the Rietveld refinement profile at 573 K. The unit cell parameters increase monotonically with temperature and the oxygen occupancy decreases with the increasing temperature from 573 to 973 K (see Table 2). Schematic 3D structures are shown in Fig. 2 for different phases.

In case of NBSCO, neutron diffraction data at room temperature was refined in the tetragonal symmetry using the setting $2a_p \times 2a_p \times 2a_p$. Fig. 3 shows the Rietveld refinement profile of NPD data at RT. Although the intensity of (1 1 1) reflection at room temperature is low, to fit superstructure reflections corresponds to HHL and HLL (H and L are odd numbers and $H \neq L$), $2a_p \times 2a_p \times 2a_p$ setting of *P4/mmm* space group was considered. Fig. 4 shows the comparison of Rietveld refinement profiles between $2a_p \times 2a_p \times 2a_p$ and $a_p \times a_p \times 2a_p$ settings at room tem-

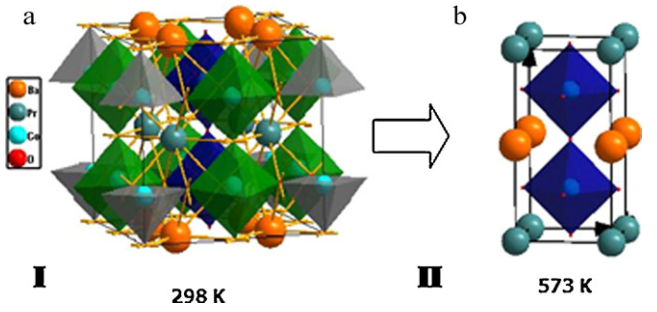


**Fig. 2.** Schematic 3D representations of structural phase changes at RT and 573 K in PBSCO and NBSCO. Cobalt atoms are located inside the octahedra, oxygens are in the corners and Pr/Nd is in 12 coordinated positions. For the sake of simplicity, the perfect order of the $2a_p \times 2a_p$ structure with 100% vacancy in 1*b* (0 0 ½) and 0% vacancy in 2*f* (0 ½0) sites are shown for the room temperature structure.

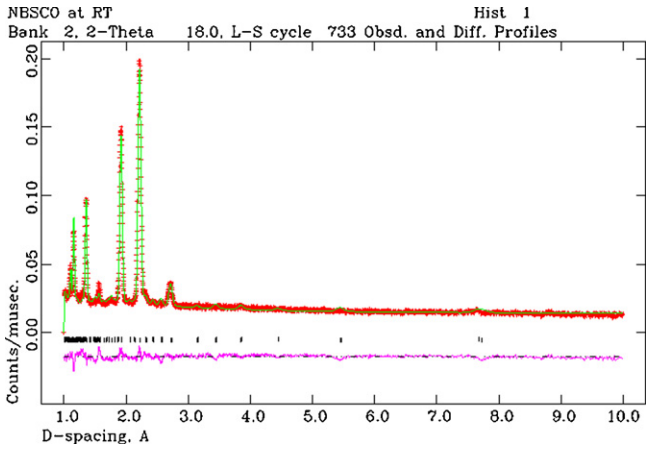


**Fig. 3.** Observed (circles) and calculated (continuous line) NPD data Rietveld refinement profile of NBSCO at RT in the *P4/mmm* space group where cell parameters are related as $2a_p \times 2a_p \times 2a_p$.

**Table 2**
Unit cell parameters, oxygen occupancies and *R*-factors of PBSCO and NBSCO at selected temperatures.

| | PBSCO | | | | NBSCO | | | |
|---|---|---|---|---|---|---|---|---|
| Parameters | RT | 100 °C | 300 °C | 700 °C | RT | 100 °C | 300 °C | 700 °C |
| Space group | *P4/mmm* | *P4/mmm* | *P4/mmm* | *P4/mmm* | *P4/mmm* | *P4/mmm* | *P4/mmm* | *P4/mmm* |
| *a* (nm) | 0.7758 (6) | 0.7683 (8) | 0.3855 (3) | 0.3908 (4) | 0.7669 (9) | 0.7678 (8) | 0.3849 (3) | 0.3893 (1) |
| *c* (nm) | 0.7704 (1) | 0.7690 (4) | 0.7729 (1) | 0.7791 (2) | 0.7685 (1) | 0.7694 (1) | 0.7725 (1) | 0.7835 (3) |
| Volume (nm$^3$) | 0.4637 (3) | 0.4540 (5) | 0.1148 (1) | 0.1190 (2) | 0.4520 (3) | 0.4536 (2) | 0.1144 (1) | 0.1187 (1) |
| $\delta$ | 0.498 | 0.6627 | 0.762 | 0.502 | 0.235 | 0.245 | 0.986 | 0.787 |
| Rp (%) | 5.31 | 7.23 | 7.98 | 3.94 | 8.07 | 8.44 | 3.08 | 3.35 |
| Rwp (%) | 4.34 | 6.37 | 6.09 | 5.35 | 7.56 | 7.95 | 3.96 | 4.27 |

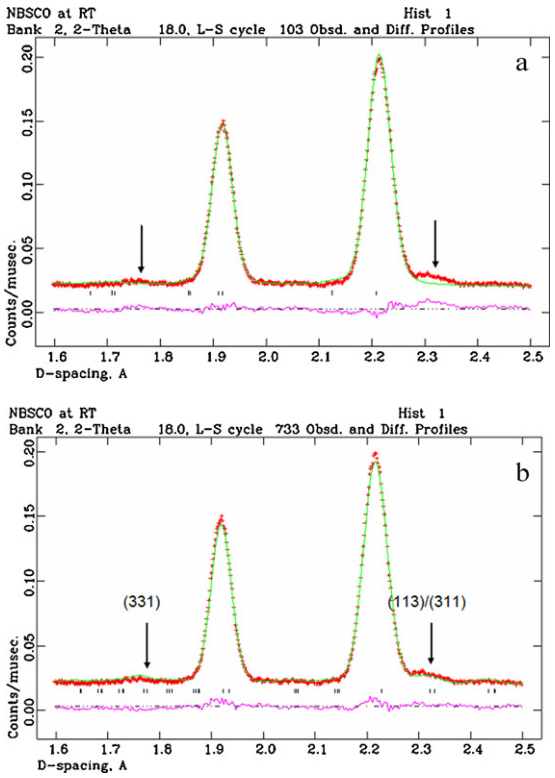


**Fig. 4.** (a) Refinement of NBSCO in $a_p \times a_p \times 2a_p$ (b) refinement of NBSCO in $2a_p \times 2a_p \times 2a_p$. Arrows shows the (1 1 3)/(3 1 1) and (3 3 1) reflection position.

perature. Arrows shows the unindexed (1 1 3)/(3 1 1) and (3 3 1) reflections in $a_p \times a_p \times 2a_p$ setting. Oxygen vacancies were distributed on the 1*b* (0 0 ½), 1*d* (½ ½ ½) and 2*f* (0 ½0) positions. It was observed that the oxygen positions at 1*b* (0 0 ½) was completely vacant and, 1*d* (½ ½ ½) and 2*f* (0 ½0) are partially occupied. Unit cell parameters, oxygen occupancies and *R*-factors of PBSCO and NBSCO at selected temperatures are given in Table 2. At 373 K, all the three Wyckoff positions for oxygen at 1*b* (0 0 ½), 1*d* (½ ½ ½) and 2*f* (0 ½0) were partially occupied. In the temperature range 473 K to 973 K, the structure is tetragonal in the *P4/mmm* space group with $a = b \approx a_p$ and $c \approx 2a_p$ and the unit cell parameters increase monotonically with temperature.

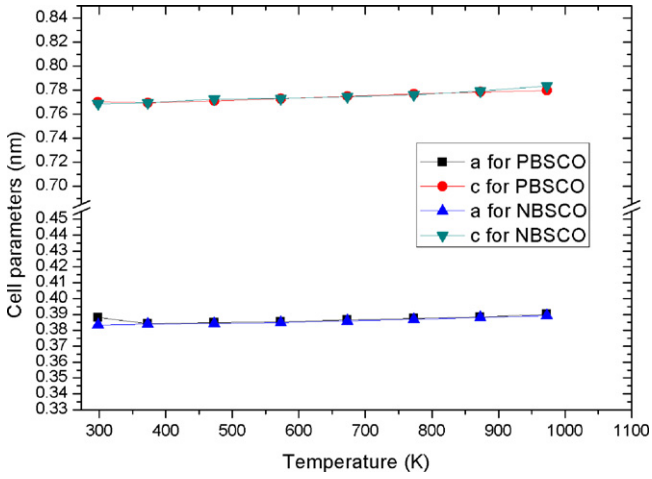


**Fig. 5.** Plot of unit cell parameters *a* and *c* versus temperature for PBSCO and NBSCO. For some of the temperatures (ordered) cell parameter *a* has been divided by 2 for simplicity.

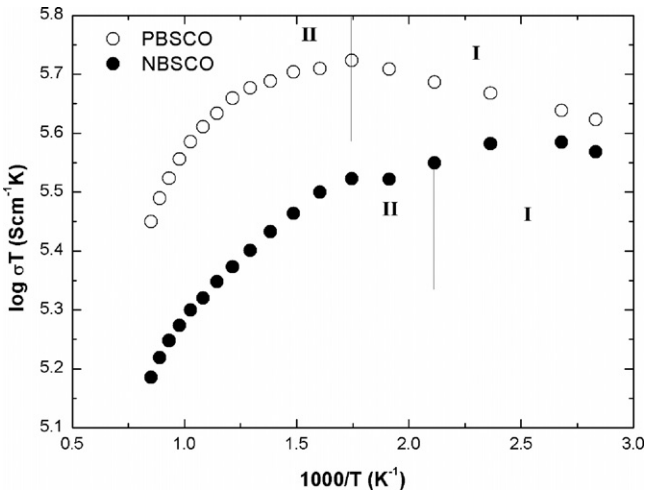


**Fig. 6.** Plot of log of conductivity versus temperature in PBSCO and NBSCO. Regions I and II are indicated in relation to structural phase changes.

Fig. 5 shows the variation of unit cell parameters with temperature of PBSCO and NBSCO. In PBSCO, small decrease in unit cell parameters was observed from RT to 373 K. From room temperature to 373 K, the oxygen occupancy increases. For a small increase in temperature, oxygen vacancy ordering decreases and more oxygen can be accommodated in the structure. Due to the thermal expansion, the unit cell parameters *a* and *c* and unit cell volume ($v$) increases with increasing temperature from 573 to 973 K. The unit cell volume increases systematically with temperature. From 573 K to 973 K, oxygen occupancy decreases with increasing temperature; the total oxygen loss is about 0.25 O/f.u and 0.37 O/f.u. for PBSCO and NBSCO, respectively. In NBSCO, unit cell parameter increases from RT to 373 K.

### 3.2. Electrical properties

The electrical conductivity of the materials was measured in order to investigate their potential as cathodes in high temperature fuel cells. Fig. 6 shows the log of electrical conductivity versus temperature plot measured from 353 K to 1173 K. The decrease of electrical conductivity with increasing temperature suggests the metallic behaviour of the material. In PBSCO, the observed conductivities were 1188 S cm$^{-1}$, 493 S cm$^{-1}$ and 240 S cm$^{-1}$ at 353 K, 873 K and 1173 K, respectively. Similarly, in NBSCO the observed conductivities were 1029 S cm$^{-1}$, 255 S cm$^{-1}$ and 131 S cm$^{-1}$ at 373 K, 873 K and 1173 K, respectively. The lowest electrical conductivities of PBSCO and NBSCO at 1173 K are still 240 S cm$^{-1}$ and 131 S cm$^{-1}$, respectively, and therefore the materials are adequate for application as a cathode in IT-SOFC. The oxygens become disordered as well as mobile at high temperatures (573–973 K). The high oxygen ion conductivity is another key property for cathodes. The apparent metallic conductivity behaviour of PBSCO above 573 K and NBSCO above 473 K may relate to an energy band overlap between Co-3d and O-2p [22,27] and the presence of $Co^{4+}$ ions from thermally generated charge disproportion of $Co^{3+}$. It also relates to the oxygen reorientation and oxygen loss on heating as this is observed to occur above 573 and 473 K for PBSCO and NBSCO, respectively (region II, Fig. 6). Two different regions have been indicated in relation to the structural phase changes in PBSCO and NBSCO (see Fig. 2). In PBSCO, region I is related to the room temperature structure with ordered oxygen vacancies and region II is related to the structure with oxygen disorder (from 573 to 973 K). The changes in conductivity and relation to the electronic orbital ordering leading to metal–insulator transition were also observed in

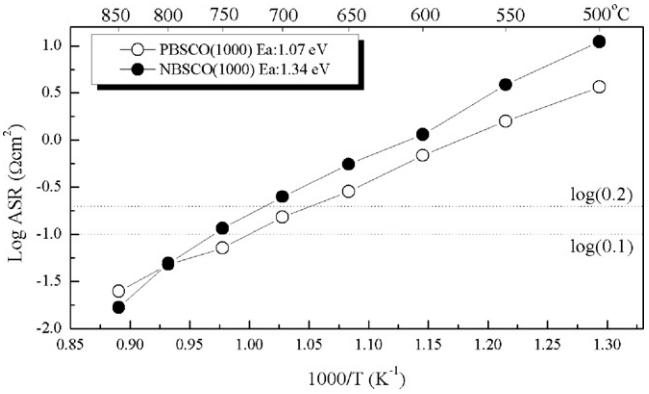


**Fig. 7.** ASR versus temperature plot for the symmetrical cell measurement using CGO91 electrolyte.

the related phases $SmBaCo_2O_{5+\delta}$ [22], $YBaCo_2O_{5+\delta}$ [2], $GdBaCo_2O_{5.5}$ [28].

Fig. 7 shows the Arrhenius plot of area specific resistance versus temperature of the symmetrical cell measured in air. The measured value of ASR was 0.286 Ω cm$^2$ and 1.15 Ω cm$^2$ at 873 K for PBSCO and NBSCO, respectively. The calculated activation energies from Arrhenius plots were 1.07 eV and 1.34 eV for PBSCO and NBSCO, respectively. This value compares well with the ASR and activation energy values of GBCO reported by Chang et al. [11]. The low value of ASR and activation energy may be related to the fast oxygen diffusion in the bulk and high kinetics on the surface of electrode [12].

## 4. Conclusions

The main objective of this research is to investigate the temperature dependent electrical and structural properties of $PrBa_{0.5}Sr_{0.5}Co_2O_{5+\delta}$ (PBSCO) and $NdBa_{0.5}Sr_{0.5}Co_2O_{5+\delta}$ (NBSCO). At room temperature PBSCO and NBSCO contains oxygen vacancies in the [$PrO_\delta$] and [$NdO_\delta$] layers and form $2a_p \times 2a_p \times 2a_p$ superstructure based on the ordering of these oxygen anions along with the cation layers. Both the structures were analysed to be tetragonal in the *P4/mmm* space group. With the increase of temperature, the oxygen vacancy ordering decreases. The oxygen occupancy increases from RT to 573 K and decreases from 573 to 973 K. Electrical conductivity in air increases from RT to 573 K for PBSCO and from RT to 473 K for NBSCO. Above these temperatures electrical conductivity decreases with increasing temperature, indicate the metallic behaviour and related to the structural change of $a_p \times a_p \times 2a_p$ type in the tetragonal symmetry. The electrical conductivity was higher than 240 S cm$^{-1}$ and 131 S cm$^{-1}$ over the entire temperature range (353–1173 K). AC impedance measurements in symmetrical cell arrangement with CGO91 electrolyte shows that ASR decreases with increasing temperature. The ASR values were 0.286 Ω cm$^2$ and 1.15 Ω cm$^2$ at 873 K for PBSCO and NBSCO, respectively.

## Acknowledgements

The authors are grateful for the financial support given by the Engineering and Physical Sciences Research Council (EPSRC) in United Kingdom and for neutron beam time from ISIS, Rutherford Appleton Laboratory.

## References

[1] A. Maignan, C. Martin, D. Pelloquin, N. Nguyen, B. Raveau, J. Solid State Chem. 142 (1999) 247.
[2] A. McKinlay, P. Connor, J.T.S. Irvine, W. Zhou, J. Phys. Chem. C 111 (51) (2007) 19120.
[3] C. Frontera, J.L. Gacia-Munoz, A.E. Carrillo, C. Ritter, D.M. Marero, A. Caneiro, Phys. Rev. B 70 (2004) 184428.
[4] T. Vogt, P.M. Woodword, P. Karen, B.A. Hunter, P. Henning, A.R. Moodenbaugh, Phys. Rev. Lett. 84 (2000) 2969.
[5] E. Surad, F. Fauth, V. Caignaert, I. Mirebeau, G. Baldinozzi, Phys. Rev. B 61 (2000) R11871.
[6] Y. Moritomo, T. Akimoto, M. Takeo, A. Machida, E. Nishibori, M. Takata, M. Sakata, K. Ohoyama, A. Nakamura, Phys. Rev. B 61 (2000) 325, R13.
[7] C. Frontera, J.L. Garcia-Munoz, A. Llobet, M.A.G. Aranda, Phys. Rev. B 65 (2002) 180405.
[8] F. Fauth, E. Surad, V. Caignaert, I. Mirebeau, Phys. Rev. B 66 (2002) 184421.
[9] A.A. Taskin, A.N. Lavrov, Y. Ando, Phys. Rev. Lett. 90 (2003) 227201.
[10] A.A. Taskin, A.N. Lavrov, Y. Ando, Appl. Phys. Lett. 86 (2005) 091910.
[11] A. Chang, S.J. Skinner, J.A. Kilner, Solid State Ionics 177 (2006) 2009.
[12] G. Kim, S. Wang, A.J. Jacobson, L. Reimus, P. Brodersen, C.A. Mims, J. Mater. Chem. 17 (2007) 2500.
[13] F. Fauth, E. Surad, V. Caigneart, B. Domenges, I. Mirebeau, L. Keller, Eur. J. Phys. B 21 (2000) R11871.
[14] D. Akahoshi, Y. Ueda, J. Solid State Chem. 156 (2001) 355.
[15] J.F. Mitchell, J. Burley, S. Short, J. Appl. Phys. 93 (2003) 7364.
[16] D.D. Khalyavin, S.N. Barilo, S.V. Shiyacv, G.L. Bynchkov, I.O. Troyanchuk, A. Furrer, A. Allenspach, H. Szymczak, R. Szymczak, Phys. Rev. B 67 (2003) 214421.
[17] C. Martin, A. Maignan, D. Pelloquin, N. Nyguen, B. Raveau, Appl. Phys. Lett. 71 (1997) 1421.
[18] O.I. Troyanchuk, N.V. Kasper, D.D. Khalyavin, H. Szymczak, R. Szymczak, M. Baran, Phys. Rev. Lett. 80 (1998) 3380.
[19] A. Maignan, V. Caigneart, B. Raveau, D. Khomskii, G. Swatzsky, Phys. Rev. Lett. 93 (2004) 026401.
[20] W. Zhou, Chem. Mater. 6 (1994) 441.
[21] J.C. Burley, J.F. Mitchell, S. Short, D. Miller, Y. Tang, J. Solid State Chem. 170 (2003) 339.
[22] J.-H. Kim, Y. Kim, P.A. Connor, J.T.S. Irvine, J. Bae, W. Zhou, J. Power Sources 194 (2009) 704.
[23] J.-H. Kim, F. Prado, A. Manthirama, J. Electrochem. Soc. 155 (2008) B1023.
[24] J.-H. Kim, A. Manthirama, J. Electrochem. Soc. 155 (2008) B385.
[25] J.H. Kim, M. Cassidy, J.T.S. Irvine, J. Bae, J. Electrochem. Soc. 156 (2009) B682.
[26] A.C. Larson, R.B.V. Dreele, Technical Report LANSCE, MSH805 Los Alamos National Laboratory, 1985.
[27] M. Ji-Woong, M. Yoshitake, S. Won-Seon, K. Kunihito, Mater. Sci. Eng. B85 (2001) 70.
[28] C. Frontera, J.L. Garcia-Munoz, A. Llobet, M.A.G. Aranda, J. Rodriguez-Carvajal, M. Respaud, J.M. Broto, B. Raquet, H. Rakoto, M. Goiran, J. Alloys Compd. 468 (2001) 323.